OPEN ACCESS
JOURNAL OF ADVANCED DIELECTRICS
Vol. 13, No. 3 (2023) 2350008 (9 pages)

DOI: 10.1142/S2010135X2350008X

High recoverable energy storage density of $Na_{0.5}Bi_{0.5}TiO_3$ lead-free ceramics modified by $Bi(Mg_{0.5}Hf_{0.5})O_3$

Kaiyuan Wang, Wenhua Li*, Xingui Tang, Siyuan Zhang, Yansong Zhang, Jia Hu, Zhihao Shen, Yanping Jiang and Xiaobin Guo

School of Physics & Optoelectronic Engineering
Guangdong University of Technology, Guangzhou Higher Education Mega Center
Guangzhou 510006, P. R. China

*liwenhuat@gdut.edu.cn

Received 13 December 2022; Revised 23 January 2023; Accepted 28 February 2023; Published 7 April 2023

Enhancing the availability and reliability of dielectric ceramic energy storage devices is of great importance. In this work, (1–x) $Na_{0.5}Bi_{0.5}TiO_3$–$x$$Bi(Mg_{0.5}Hf_{0.5})O_3$ (NBT–xBMH) lead-free ceramics were created utilizing a solid-state reaction technique. All NBT–xBMH ceramics have a single perovskite structure. With increasing BMH doping, the grain size shrinks drastically, which greatly enhances the breakdown electric field (310 kV/cm at x = 0.25). Additionally, the relaxation behaviors of NBT–xBMH ceramics with high BMH content are more remarkable. Among all designed components, the NBT–0.25BMH ceramic exhibits the best energy storage performance with a high W_{rec} of 4.63 J/cm^3 and an η of 75.1% at 310 kV/cm. The NBT–0.25BMH ceramic has exceptional resistance to fluctuations in both frequency (5–500 Hz) and temperature (30–100°C). Charge–discharge test shows that the NBT–0.25BMH ceramic has a quick discharge rate ($t_{0.9}$ < 110 ns). With these properties, the NBT–0.25BMH ceramic may have applications in microdevices as well as in ultra-high power electronic systems.

Keywords: Lead-free ceramic; energy storage; $Bi(Mg_{0.5}Hf_{0.5})O_3$; dielectric properties.

1. Introduction

Recently, the popularity of pulse power technology and the increasing demand for miniaturized devices have led to an increasing requirement for capacitors with large energy storage capacities.[1–3] Dielectric energy storage capacitors with a large power density and a short charge–discharge cycle meet the demands of ultra-high power electronic systems.[4–6] Compared with most dielectric energy storage materials, dielectric ceramics have the merits of higher dielectric constant, lower dielectric loss, moderate breakdown electric field, better temperature stability, and good fatigue resistance.[7–10] Thus, dielectric energy storage ceramic materials have a broad application prospect in heat-resistant dielectric pulse systems. Nevertheless, the poor energy storage density hinders their practical applicability.[1,7] Therefore, it is necessary to deeply study and optimize the energy storage capacity and reliability of dielectric ceramics.

The total energy density (W), recoverable energy density (W_{rec}), energy loss density (W_{loss}), and energy storage efficiency (η) of dielectric ceramics can be determined based on their polarization–electric field (P–E) loops. The corresponding mathematical equations are given as follows[11,12]:

$$W = \int_0^{P_{max}} EdP, \tag{1}$$

$$W_{rec} = \int_{P_r}^{P_{max}} EdP, \tag{2}$$

$$W_{loss} = W - W_{rec}, \tag{3}$$

$$\eta = \frac{W_{rec}}{W} \times 100\%, \tag{4}$$

where P_{max}, P_r, and E stand for maximum polarization, remnant polarization, and electric field, respectively. According to Eqs. (1)–(4), a dielectric ceramic material with high W_{rec} is considered to have both high P_{max}, high breakdown electric field strength (BDS), and low P_r.[13]

Bi-based ferroelectric ceramic materials possess great saturation polarization strength because Bi^{3+} has a similar electronic configuration to Pb^{2+}.[7]$Na_{0.5}Bi_{0.5}TiO_3$(NBT)-ceramic hasa high P_{max} and dielectric constantandis environmentally friendly, which are potential advantages as energy storage applications. However, NBT ceramic has significant disadvantages, such as poor sintering density, weak breakdown electric field strength, many types of defects resulting from the easy volatility of Na^+ and Bi^{3+},[14] and large residual polarization intensity, which makes poor energy storage performance. Although pure NBT ceramic does not perform well in energy storage, many studies have identified that the

*Corresponding author.

capacity and reliability of energy storage can be strengthened by the construction of multiple systems, doping with ionic, optimization of sintering processes, etc.[15–17] Some scholars have studied introducing other ferroelectrics with a perovskite structure (e.g., $BaTiO_3$(BT), $SrTiO_3$) into NBT ceramic to form a binary solid solution as a matrix and then doping it with a $Bi(M_1M_2)O_3$ type composite solid solution.[18,19] This strategy effectively reduces the P_r and coercive field strength while maintaining high BDS and P_{max}, resulting in excellent energy storage properties. Lin *et al.* achieved a W_{rec} of 3.45 J/cm^3 and an η of 88.01% in $0.85(0.7NBT–0.3SrTiO_3)–0.15Bi(Mg_{2/3}Nb_{1/3})O_3$ ceramic through a strategy of introducing the lone pair electron $6s^2$ configuration of Bi^{3+} and refining grain.[18] Guo *et al*. introduced $Bi(Mg_{2/3}Nb_{1/3})O_3$ into $0.94NBT–0.06BaTiO_3$ to produce a W_{rec} of 6.3 J/cm^3 with the design of constructing polymorphic polar nano-regions (PNRs) coexistence by phase structure control.[20] The BDS was greatly improved (reaching 522 kV/cm) by introducing $Bi(Mg_{0.5}Zr_{0.5})O_3$ into $(Na_{0.5}Bi_{0.5})_{0.65}Sr_{0.35}TiO_3$ binary solid solution, and a W_{rec} of 8.46 J/cm^3 was achieved by Zhu *et al*.[21]

There are a few reports on introducing the $Bi(M_1M_2)O_3$ type composite solid solutions into pure NBT ceramic to enhance its energy storage capabilities. In some studies, Hf^{4+} and Mg^{2+} were doped into the *B*-site of ceramics with the perovskite structure, which greatly improved the energy storage properties of the ceramics.[18–23] Therefore, these two elements are selected to be doped into the *B*-site of NBT ceramics. The $Bi(Mg_{0.5}Hf_{0.5})O_3$ (BMH) was introduced into the NBT ceramic to form NBT–*x*BMH (x = 0.00, 0.10, 0.15, 0.20, 0.25, and 0.30) ceramics. The energy storage capacity, reliability, dielectric characteristics, and microstructure of NBT–*x*BMH ceramics were investigated in detail.

2. Material and Methods

The NBT–*x*BMH ceramics were produced utilizing a solid-state reaction technique. HfO_2 (99.99%), TiO_2 (99%), Bi_2O_3 (99.99%), MgO (99.9%), and Na_2CO_3 (99.8%) were used after being dried at 75°C for 18 h. The reagents were weighed based on the stoichiometric ratios in experimental protocols, and then the mixed reagents were ball milled at 350 rpm for 24 h. Afterward, the dried powder was calcined for 3 h at 850°C and then ground and dried under the same conditions. Next, the powder was added with polyvinyl butyral which promotes granulation, and then placed in a mold and pressed into ceramic discs at 6 MPa. Finally, all the ceramic samples were obtained by sintering the ceramic discs at 1160°C in an air atmosphere for 2 h.

X-ray diffraction (XRD) patterns of the NBT–*x*BMH ceramics with polished and ultrasonically cleaned surfaces were measured using an X-ray diffractometer (D8 ADVANCE, Bruker, Germany). Dielectric properties of the ceramics sintered with silver electrodes were tested by an LCR meter (E4980A, Keysight). Microscopic morphologies of ultrasonically cleaned and gold-plated NBT–*x*BMH ceramics were investigated by scanning electron microscopy (SEM, LYRA 3 XMU, Tescan, Czech Republic). The Radiant Precision Premier (Albuquerque, NM, America) and temperature-controlled stage were used to analyze the *P–E* loops of NBT–*x*BMH ceramics polished to 120 μm and plated with gold electrodes. In a self-made RLC circuit, charge–discharge behaviors of the NBT–0.25BMH ceramic polished to 120 μm and sintered with silver electrodes were tested.

3. Results and Discussion

The XRD images of NBT–*x*BMH ceramics are illustrated in Fig. 1(a). Obviously, a single perovskite structure is present in all ceramics, which implies that NBT and BMH form solid solutions.[18] In addition, these images are consistent with similar existing reports.[22,24] The pseudo-cubic structures of the NBT–*x*BMH ceramics are demonstrated by the non splitting of the diffraction peaks.[18] From Fig. 1(b), the (110) peak slightly moves to a lower angle as the amount of BMH-doped increases, which indicates that the cell volume is gradually expanding.[13,19] This is attributed to the replacement of Ti^{4+} (0.605 Å) by the larger ions (Mg^{2+} (0.72 Å) and Hf^{4+} (0.71 Å)).

The sintering process makes the relative density and strength of the ceramic samples larger.[25,26] Figure 2 displays the SEM pictures of the surfaces of the NBT–*x*BMH ceramics. Dense microstructures were observed in all NBT–*x*BMH ceramics, and the introduction of BMH resulted in a dramatic decrease in grain size. These facilitate the improvement of BDS according to previous studies.[27,28] To further analyze the influence of BMH doping on grain size, statistical analysis of grain size was performed using Nano Measurer software, as seen in the illustrations of Fig. 2. With increasing BMH doping, the grain size decreases sharply at first, then continues to decrease slowly when $x \le 0.25$, and then increases at x = 0.30. Reasons for grain refinement are given below: (1) Doping with Bi^{3+} inhibits the volatility of Bi^{3+} and Na^+ during

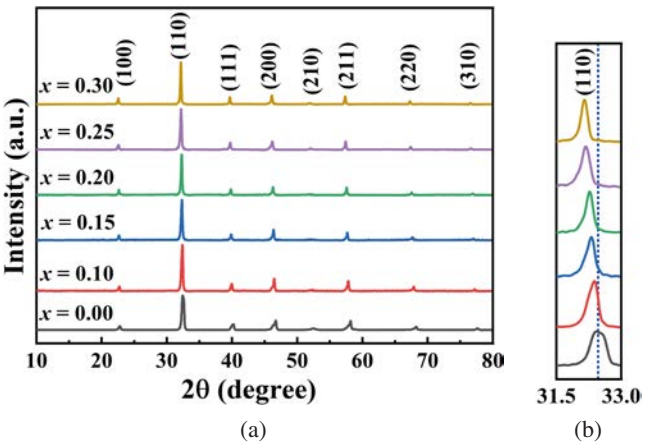

Fig. 1. (a) The XRD images of NBT–*x*BMH ceramics. (b) Magnified (110) peaks.

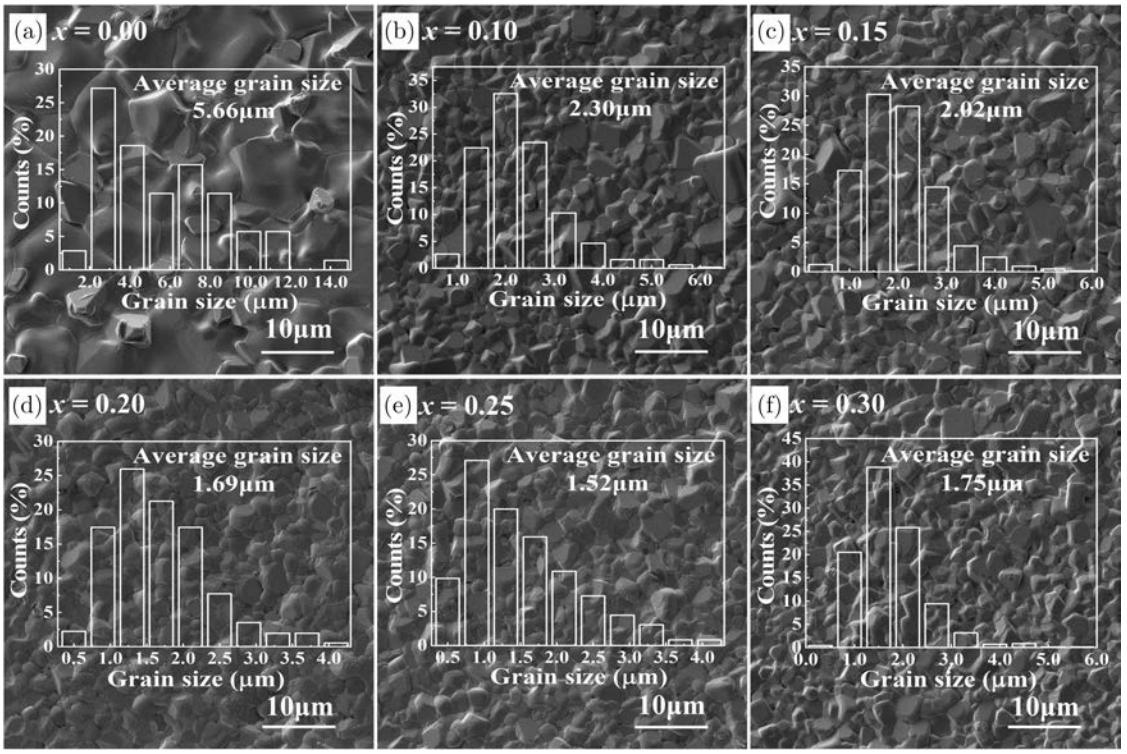

Fig. 2. SEM pictures of NBT–xBMH ceramics. The illustrations provide grain size statistics.

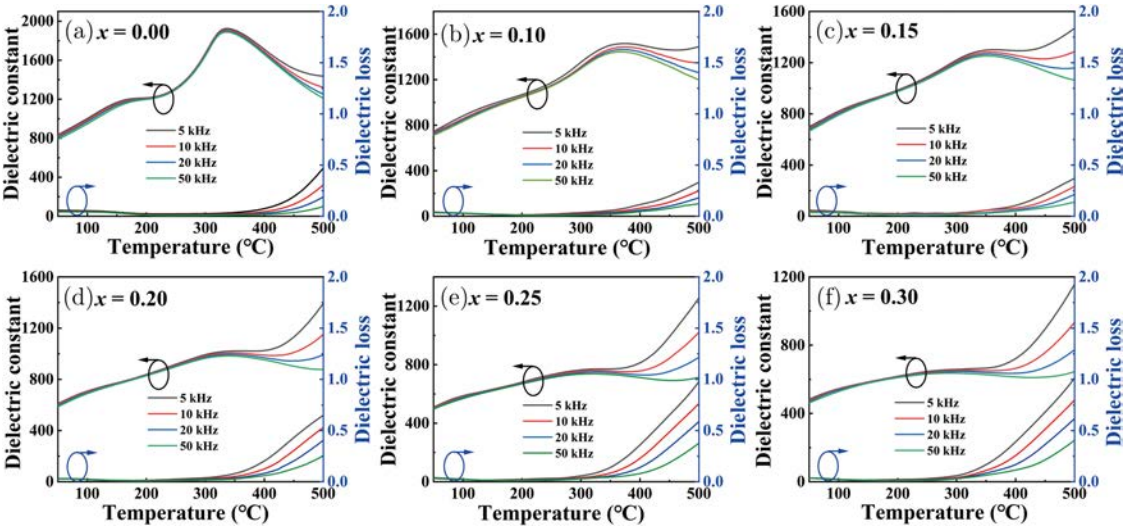

Fig. 3. Dielectric properties of NBT–xBMH ceramics from 5 kHz to 50 kHz.

sintering, thus, reducing the formation of oxygen vacancies, which facilitates the suppression of grains growth.[29] (2) The larger ions replace Ti^{4+}, increasing the lattice strain energy and obstructing grain boundary motion, which results in grainrefinement.[30] The reason for the slightly larger grain size at $x = 0.30$ is that doping with too many ions causes the creation of new vacancies which may cause the grains to grow.[21]

Figure 3 shows the temperature versus dielectric properties in NBT–xBMH ceramics. BMH-doped ceramic samples are relaxor ferroelectrics, as shown by the frequency dependence of their dielectric loss and dielectric constant.[21] Besides, all the ceramics exhibit significant high-temperature dielectric relaxation above 340°C.[31] The temperature which corresponds to the dielectric anomaly broad peak is the Curie temperature (T_m). Detailed values of the T_m and dielectric constant peak (ε_m) are provided in Table 1. As increasing BMH doping, T_m increases first and then decreases, and ε_m decreases significantly. Besides, the dielectric peaks

Table 1. Dielectric parameters of BNT–xBMH ceramics at 50 kHz.

Composition	T_m (°C)	ε_m	γ
NBT	336	1888	1.76
NBT-0.10BMH	368	1444	1.83
NBT-0.15BMH	352	1253	1.87
NBT-0.20BMH	340	982	1.89
NBT-0.25BMH	320	737	1.91
NBT-0.30BMH	288	636	1.97

gradually become blurred, forming dielectric plateaus near T_m. As a consequence, the NBT–xBMH ceramics with higher BMH content exhibit smaller dielectric constant changes near T_m, which contributes to the energy storage capability of the ceramics being stable over large temperature variations.[22,32] The values of dielectric loss of the ceramics are always nearly zero below 340°C, which facilitates the enhancement of BDS.[19] Dielectric loss increases suddenly after 340°C, which is caused by the temperature increase which results in an increase in the space charge or conductivity of the ferroelectric ceramic.[33] To further evaluate the relaxation phenomenon of the ceramics, the diffusion parameters (γ) were calculated based on the modified Curie–Weiss formula.[13,34] Figure B1 (Supporting Information) illustrates typical fitting graphs, and the γ values are presented in Table 1. Apparently, the γ value of the ceramic increases with the increasing BMH content and gradually approaches 2, indicating that the introduction of BMH is beneficial to enhance the relaxation characteristic of pure NBT ceramic.[31] Multiple cations at A-sites and B-sites are the primary reason for the enhanced relaxation effect of the ceramics.[35]

The P–E loops of NBT–xBMH ceramics are displayed in Fig. 4. Obviously, pure NBT ceramic has a high P_r and weak BDS, resulting in poor energy storage performance. The gradual thinning of the P–E loops indicates a shift in NBT–xBMH ceramics from standard ferroelectric type to relaxation type with increasing BMH doping.[57] To more intuitively observe the effect of BMH introduction on the P–E loops, Fig. 5(a) provides the P–E loops under the same electric field. The P_r and P_{max} decrease significantly with increasing BMH doping. In particular, the P_r decreases almost to zero, which is beneficial for improving energy storage efficiency. The main factor leading to reduced ferroelectric properties and smaller P_r is usually considered to be the PNRs caused by the addition of BMH. The introduction of Mg^{2+} and Hf^{4+} with different ionic radii and valences disrupts the long-range ordering of the B-site of NBT ceramic, which increases the local structural disorder of NBT ceramic samples, destroys the ferroelectric macrodomains and promotes the formation of PNRs.[20,21,58,59]

Figure 5(b) displays the η and W_{rec} of the NBT–xBMH ceramics under the critical electric field. Obviously, with increasing BMH doping, the BDS increases when $x \le 0.25$ and then decreases. Related studies have demonstrated that the BDS is intimately associated with the grain size, which can be formulated as $E_{BDS} \propto 1/\sqrt{G}$ where G represents grain size.[60–62] Combined with the previous analysis of grain size, the correlation between BDS and grain size of NBT–xBMH ceramics is in accordance with the above equation. From Fig. 5(b), NBT–0.25BMH ceramic obtained the best energy storage capabilities. The NBT–0.25BMH ceramic achieved a high W_{rec} of 4.63 J/cm^3 and an η of 75.1% at 310 kV/cm, which is a great improvement compared to the NBT ceramic (W_{rec} = 1.24 J/cm^3, η = 33.1%). Thus, significant improvements in energy storage capabilities were achieved by introducing the BMH into NBT ceramics. Figure 5(c) shows the comparison of the energy storage properties of some NBT-based, BT-based, $K_{0.5}Na_{0.5}NbO_3$ (KNN)-based, and $NaNbO_3$

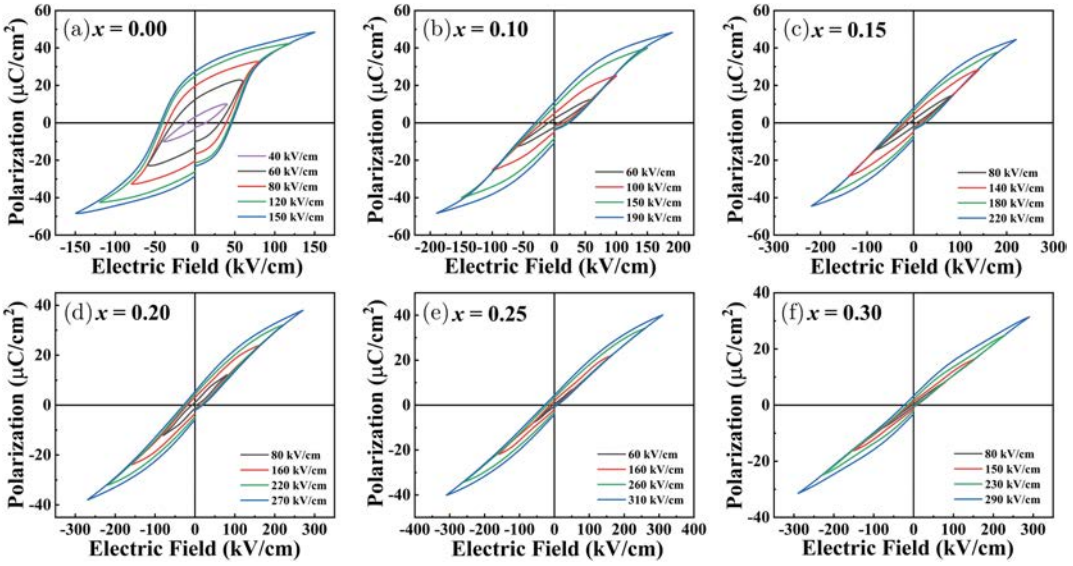

Fig. 4. P–E loops of NBT–xBMH ceramics in electric fields less than and equal to the critical electric field.

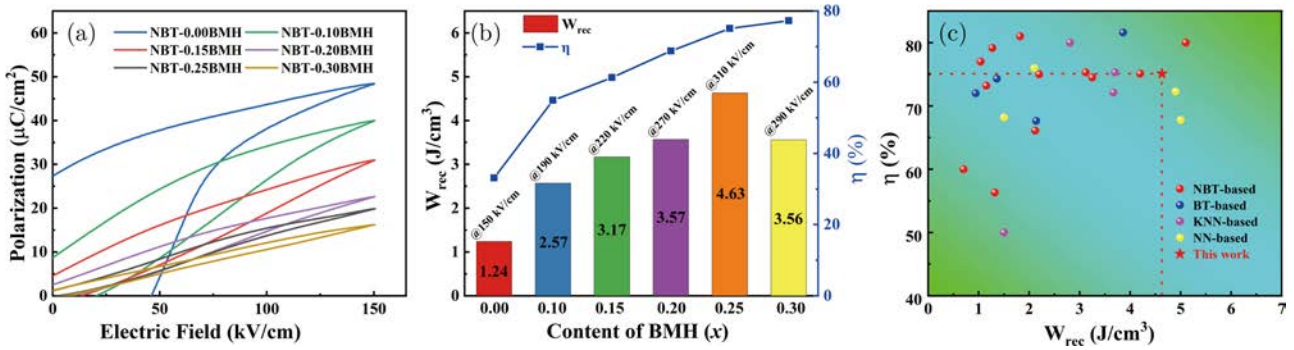

Fig. 5. (a) Unipolar *P–E* loops of NBT–*x*BMH ceramics at 150 kV/cm and 10 Hz. (b) η and W_{rec} of NBT–*x*BMH ceramics under critical electric field. (c) Comparison of energy storage properties of NBT–0.25BMH ceramic with other lead-free ceramics.[13,17,22,36–56]

(NN)-based ceramics with the NBT–0.25BMH ceramic. The NBT–0.25BMH ceramic has good overall properties compared to the other ceramics, which indicates that the optimization strategy in this work is very effective in improving the energy storage performance of NBT ceramic.

Energy storage materials often work in complex environments, so investigating the frequency stability and thermostability of the NBT–0.25BMH ceramic is of great importance. The *P–E* loops of the NBT–0.25BMH ceramic at different frequencies (5–500 Hz) are presented in Fig. 6(a). The loops only have a small variation in the frequency range. As depicted in Fig. 6(b), the W_{rec} varies from 1.80 J/cm^3 to 1.98 J/cm^3 and the η varies from 80.2% to 87.9%, corresponding to a variation of 9.7% and 9.6%, respectively. The performance of energy storage changes little with changes of frequency, so the NBT–0.25BMH ceramic has good frequency stability. Figures 6(c) and 6(d) show the *P–E* loops at various temperatures (30–100°C) and the corresponding calculated η and W_{rec} of the NBT–0.25BMH ceramic, respectively. The loops are very slim, and the η and W_{rec} fluctuate mildly around 85.4% and 1.91 J/cm^3, respectively. Their corresponding variation rates are only 1.6% and 2.3%, respectively. Thus, the NBT–0.25BMH ceramic possesses favorable thermal stability against changes in the external environment.

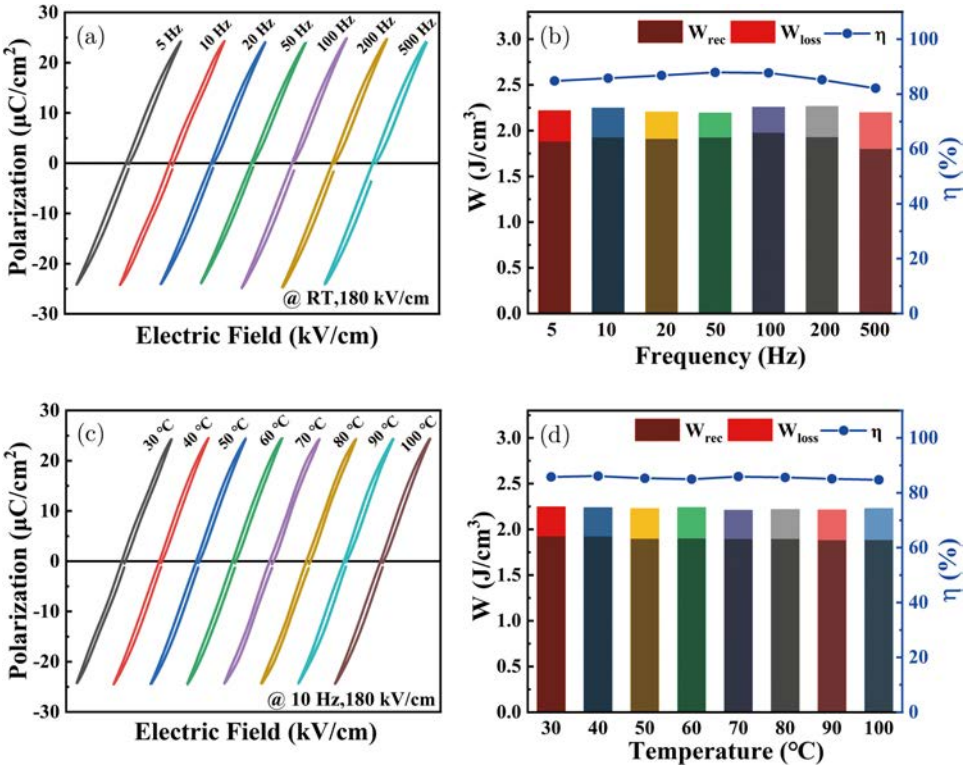

Fig. 6. (a) and (c) are the variations of *P–E* loops at different frequencies (5–500 Hz) and temperatures (30–100°C) of the NBT–0.25BMH ceramic, respectively. (b) and (d) are W_{rec}, η, and W_{loss} calculated from (a) and (c), respectively.

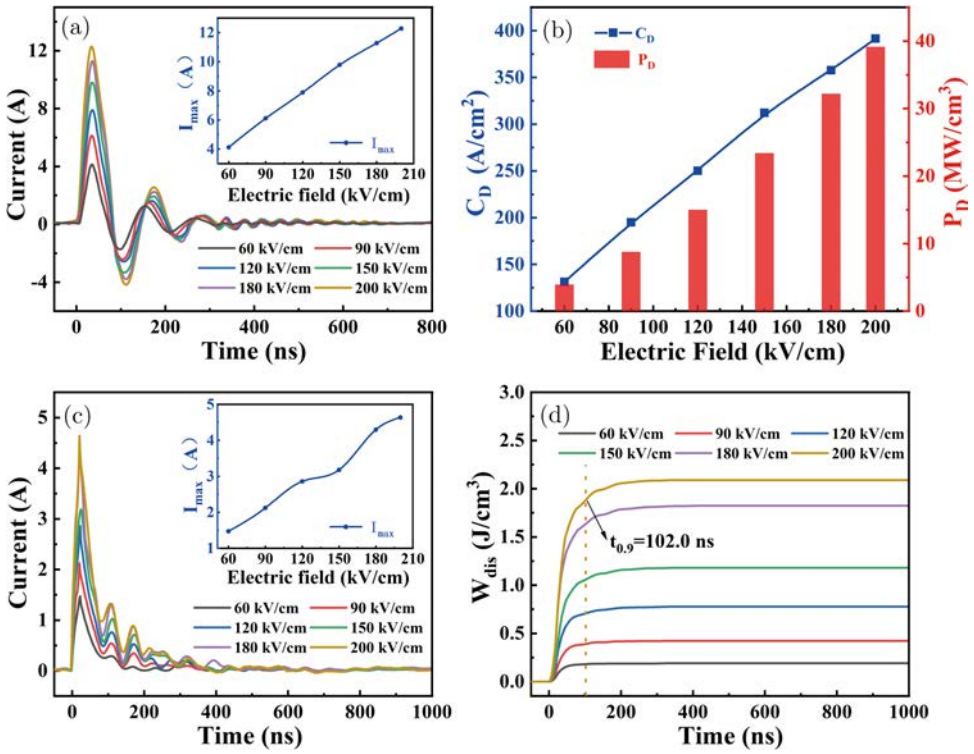

Fig. 7. (a) and (c) are underdamped discharge current waveforms and overdamped discharge current waveforms of the NBT–0.25BMH ceramic, respectively. (b) Variations of P_D and C_D with the electric field for the NBT–0.25BMH ceramic. (d) The calculated W_{dis} changes with time.

The pulse charge–discharge test measures the performance of ceramic capacitors in actual use, and the test results are more informative than the results of W_{rec} in practical applications. Figure 7(a) displays current waveforms of underdamped discharge for the NBT–0.25BMH ceramic. The current waveforms only need 500 ns to complete several oscillations. The first current peak (I_{max}) increases from 4.12 A to 12.29 A with rising voltage, as seen in the illustration of Fig. 7(a). The current density (C_D) and power density (P_D) of NBT–0.25BMH ceramic gradually increase with increasing voltage, reaching 391.4 A/cm^2 and 39.1 MW/cm^3, respectively.

The current waveforms of over damped discharge for the NBT–0.25BMH ceramic are depicted in Fig. 7(c). Obviously, the waveform peaks occur in less than 50 ns, and the discharge process is finished in about 500 ns. The illustration in Fig. 7(c) displays that the I_{max} value grows from 1.48 A to 4.64 A. Discharge energy density (W_{dis}) is estimated by Eq. (5).[63]

$$W_{dis} = R\int i^2(t)dt/V, \tag{5}$$

where R is the load resistance (205 Ω) and V is the volume of the NBT–0.25BMH ceramic. The variation of W_{dis} with time is presented in Fig. 7(d). Notably, the actual energy discharged by the NBT–0.25BMH ceramic under 200 kV/cm electric field (W_{dis} = 2.09 J/cm^3) is smaller than the energy calculated from Eq. (3) (W_{rec} = 2.28 J/cm^3). This may be caused by the differences in the characterization mechanisms for the static P–E hysteresis test which was performed at a frequency of 10 Hz (corresponding to 0.1 s) in this study, and the dynamic charge–discharge test which was performed on a time scale close to microseconds or sub-microseconds.[64] In the charge–discharge test, the energy was not completely released because the ferroelectric domains could not be converted in time due to the fast discharge speed.[65] Besides, the equivalent series resistance in the circuit also consumed part of the energy.[2] Generally, $t_{0.9}$ refers to the time taken for W_{dis} to reach 90% of its maximum.[66] The $t_{0.9}$ of NBT–0.25BMH ceramic is always small (less than 110 ns) under the different electric fields. In summary, the NBT–0.25BMH ceramic shows excellent discharge capability which facilitates its application in pulsed power devices.

4. Conclusions

The NBT–xBMH ceramics were successfully created, and the detailed mechanisms related to the dielectric properties and energy storage performance were analyzed. With increasing BMH doping, the size of the grains dropped sharply, and the relaxation performance was enhanced. Furthermore, the P_r of the ceramic samples with high doping content decreased sharply, and the BDS was greatly improved. Thus, the NBT–0.25BMH ceramic obtained good energy storage performance

(W_{rec} = 4.63 J/cm^3, η = 75.1%). In addition, the ceramic exhibited outstanding thermostability, good frequency stability, and a very quick discharge rate. These properties make NBT–0.25BMH ceramic potential for applications in energy storage devices.

Acknowledgments

This work was supported by the National Natural Science Foundation of China (Grant Nos. 51604087, 11904056, and 12172093), the Guangdong Basic and Applied Basic Research Foundation (Grant No. 2021A1515012607).

References

[1]H. Du, Z. Yang, F. Gao, L. Jin, H. Cheng and S. Qu, Lead-free nonlinear dielectric ceramics for energy storage applications: Current status and challenges, *J. Inorg. Mater.* **33**, 1046 (2018).

[2]Y. Huang, F. Li, H. Hao, F. Xia, H. Liu and S. Zhang, $(Bi_{0.51}Na_{0.47})$-TiO_3 based lead free ceramics with high energy density and efficiency, *J. Materiomics* **5**, 385 (2019).

[3]T. Wang, Y. Wang, H. Yang, Y. Lin, L. Kong, S. Gao and F. Wang, Structure, dielectric properties of low-temperature-sintering $BaTiO_3$-based glass–ceramics for energy storage, *J. Adv. Dielectr.* **8**, 1850041 (2018).

[4]P. Ge, X. Tang, K. Meng, X. Huang, Q. Liu, Y. Jiang, W. Gong and T. Wang, Ultrahigh energy storage density and superior discharge power density in a novel antiferroelectric lead hafnate, *Mater. Today Phys.* **24**, 100681 (2022).

[5]K. Meng, W. Li, X. Tang, Q. Liu and Y. Jiang, A review of a good binary ferroelectric ceramic: $BaTiO_3$–$BiFeO_3$, *ACS Appl. Electron. Mater.* **4**, 2109 (2022).

[6]X. Hao, A review on the dielectric materials for high energy-storage application, *J. Adv. Dielectr.* **3**, 1330001 (2013).

[7]L. Li, P. Fan, M. Wang, N. Takesue, D. Salamon, A. N. Vtyurin, Y. Zhang, H. Tan, B. Nan, Y. Lu, L. Liu and H. Zhang, Review of lead-free Bi-based dielectric ceramics for energy-storage applications, *J. Phys. D*: *Appl. Phys.* **54**, 293001 (2021).

[8]W. Wang, X. Tang, Y. Jiang, Q. Liu, W. Li, X. Guo and Z. Tang, Modified relaxor ferroelectrics in $BiFeO_3$-$(Ba,Sr)TiO_3$-$BiScO_3$ ceramics for energy storage applications, *Sustain. Mater. Technol.* **32**, e00428 (2022).

[9]Z. Yang, H. Du, L. Jin and D. Poelman, High-performance lead-free bulk ceramics for electrical energy storage applications: Design strategies and challenges, *J. Mater. Chem. A* **9**, 18026 (2021).

[10]S. Zhang, W. Li, Y. Zhang, X. Tang, Y. Jiang and X. Guo, Large energy density and high efficiency achieved simultaneously in $Bi(Mg_{0.5}Hf_{0.5})O_3$-modified $NaNbO_3$ ceramics, *Results Phys.* **44**, 106194 (2023).

[11]R. Kang, Z. Wang, W. Yang, X. Zhu, P. Shi, Y. Gao, P. Mao, J. Zhao, L. Zhang and X. Lou, Extraordinary energy storage performance and thermal stability in sodium niobate-based ceramics modified by the ion disorder and stabilized antiferroelectric orthorhombic *R* phase, *J. Mater. Chem. A* **9**, 24387 (2021).

[12]R. Vandana, R. P. Gupta, M. Tandon and M. Tomar, Electrocaloric and energy storage properties of sol-gel derived lanthanum doped PZT thick films, *Mater. Sci. Semicond. Process.* **150**, 106970 (2022).

[13]K. Meng, W. Li, X. Tang, Q. Liu and Y. Jiang, The defect related energy-storage properties of A-site off-stoichiometry ferroelectric ceramic, *Appl. Phys. A-Mater.* **127**, 337 (2021).

[14]R. Bhattacharyya and S. Omar, Electrical conductivity study of *B*-site Ga doped non-stoichiometric sodium bismuth titanate ceramics, *J. Alloys Compd.* **746**, 54 (2018).

[15]J. Lv, Q. Li, Y. Li, M. Tang, D. Jin, Y. Yan, B. Fan, L. Jin and G. Liu, Significantly improved energy storage performance of NBT-BT based ceramics through domain control and preparation optimization, *Chem. Eng. J.* **420**, 129900 (2021).

[16]M. Munir, M. Habib, S. A. Khan, M.-H. Kim, S. Lee, T.-K. Song, A. H. Baluch, A. Turak and A. Hussain, Energy storage and piezoelectric properties of lead-free $SrTiO_3$-modified $0.965Bi_{0.5}$-$Na_{0.5}TiO_3$–$0.035BaTiO_3$ ceramics, *J. Mater. Sci.*: *Mater. Electron.* **32**, 10712 (2021).

[17]Y. Zhang, W. Li, X. Tang, K. Meng, S. Zhang, X. Xiao, X. Guo, Y. Jiang and Z. Tang, Energy storage and charge–discharge performance of *B*-site doped NBT-based lead-free ceramics, *J. Alloys Compd.* **911**, 165074 (2022).

[18]Y. Lin, D. Li, M. Zhang and H. Yang, $(Na_{0.5}Bi_{0.5})_{0.7}Sr_{0.3}TiO_3$ modified by $Bi(Mg_{2/3}Nb_{1/3})O_3$ ceramics with high energy-storage properties and an ultrafast discharge rate, *J. Mater. Chem. C* **8**, 2258 (2020).

[19]Y. Qiu, Y. Lin, X. Liu and H. Yang, $Bi(Mg_{2/3}Nb_{1/3})O_3$ addition inducing high recoverable energy storage density in lead-free $0.65BaTiO_3$-$0.35Bi_{0.5}Na_{0.5}TiO_3$ bulk ceramics, *J. Alloys Compd.* **797**, 348 (2019).

[20]B. Guo, Y. Yan, M. Tang, Z. Wang, Y. Li, L. Zhang, H. Zhang, L. Jin and G. Liu, Energy storage performance of $Na_{0.5}Bi_{0.5}TiO_3$ based lead-free ferroelectric ceramics prepared via non-uniform phase structure modification and rolling process, *Chem. Eng. J.* **420**, 130475 (2021).

[21]X. Zhu, Y. Gao, P. Shi, R. Kang, F. Kang, W. Qiao, J. Zhao, Z. Wang, Y. Yuan and X. Lou, Ultrahigh energy storage density in $(Bi_{0.5}Na_{0.5})_{0.65}Sr_{0.35}TiO_3$-based lead-free relaxor ceramics with excellent temperature stability, *Nano Energy* **98**, 107276 (2022).

[22]L. Zhang, Y. Pu, M. Chen, T. Wei, W. Keipper, R. Shi, X. Guo, R. Li and X. Peng, High energy-storage density under low electric fields and improved optical transparency in novel sodium bismuth titanate-based lead-free ceramics, *J. Eur. Ceram. Soc.* **40**, 71 (2020).

[23]R. Kang, Z. Wang, Y. Zhao, Y. Li, Y. Hu, X. Hao, L. Zhang and X. Lou, Enhanced energy storage performance of $Bi_{0.5}K_{0.5}TiO_3$-based ceramics via composition modulation, *J. Alloys Compd.* **935**, 167999 (2023).

[24]M. Dunce, E. Birks, M. Antonova, L. Bikse, S. Dutkevica, O. Freimanis, M. Livins, L. Eglite, K. Smits and A. Sternberg, Influence of sintering temperature on microstructure of $Na_{0.5}Bi_{0.5}TiO_3$ ceramics, *J. Alloys Compd.* **884**, 160955 (2021).

[25]Y. Liu, Z. Li, H. Thong, J. Lu, J. Li, W. Gong and K. Wang, Grain size effect on piezoelectric performance in perovskite-based piezoceramics, *Acta Phys. Sin.* **69**, 217704 (2020).

[26]M. N. Rahaman, *Ceramic Processing and Sintering*, 2nd edn. (CRC Press, USA, 2003).

[27]X. Qiao, D. Wu, F. Zhang, B. Chen, X. Ren, P. Liang, H. Du, X. Chao and Z. Yang, $Bi_{0.5}Na_{0.5}TiO_3$-based relaxor ferroelectric ceramic with large energy density and high efficiency under a moderate electric field, *J. Mater. Chem. C* **7**, 10514 (2019).

[28]A. Xie, H. Qi and R. Zuo, Achieving remarkable amplification of energy-storage density in two-step sintered $NaNbO_3$–$SrTiO_3$-antiferroelectric capacitors through dual adjustment of local heterogeneity and grain scale, *ACS Appl. Mater. Interfaces* **12**, 19467 (2020).

[29]X. Zhu, P. Shi, R. Kang, S. Li, Z. Wang, W. Qiao, X. Zhang, L. He, Q. Liu and X. Lou, Enhanced energy storage density of $Sr_{0.7}Bi_xTiO_3$ lead-free relaxor ceramics via *A*-site defect and grain size tuning, *Chem. Eng. J.* **420**, 129808 (2021).

[30]C. Luo, Q. Feng, N. Luo, C. Yuan, C. Zhou, Y. Wei, T. Fujita, J. Xu and G. Chen, Effect of Ca^{2+}/Hf^{4+} modification at A/B sites on energy-storage density of $Bi_{0.47}Na_{0.47}Ba_{0.06}TiO_3$ ceramics, *Chem. Eng. J.* **420**, 129861 (2021).

[31]Y. Zhang, W. Li, S. Zhang, X. Tang, Q. Liu, Y. Jiang, Z. Tang and X. Guo, The dielectric relaxation and impedance spectroscopy analysis of $(Bi_{0.5}Na_{0.5})TiO_3$-based ceramics, *Mater. Res. Bull.* **153**, 111874 (2022).

[32]P. Chen and B. Chu, Improvement of dielectric and energy storage properties in $Bi(Mg_{1/2}Ti_{1/2})O_3$-modified $(Na_{1/2}Bi_{1/2})_{0.92}Ba_{0.08}TiO_3$ ceramics, *J. Eur. Ceram. Soc.* **36**, 81 (2016).

[33]O. Bidault, P. Goux, M. Kchikech, M. Belkaoumi and M. Maglione, Space-charge relaxation in perovskites, *Phys. Rev. B* **49**, 7868 (1994).

[34]N. Truong-Tho and L. D. Vuong, Effect of sintering temperature on the dielectric, ferroelectric and energy storage properties of SnO_2-doped $Bi_{0.5}(Na_{0.8}K_{0.2})_{0.5}TiO_3$ lead-free ceramics, *J. Adv. Dielectr.* **10**, 2050011 (2020).

[35]G. Liu, J. Dong, L. Zhang, Y. Yan, R. Jing and L. Jin, Phase evolution in $(1–x)(Na_{0.5}Bi_{0.5})TiO_{3–x}SrTiO_3$ solid solutions: A study focusing on dielectric and ferroelectric characteristics, *J. Materiomics* **6**, 677 (2020).

[36]Q. Chai, D. Yang, X. Zhao, X. Chao and Z. Yang, Lead-free (K,Na)NbO_3-based ceramics with high optical transparency and large energy storage ability, *J. Am. Ceram. Soc.* **101**, 2321 (2018).

[37]X. Zhou, C. Yuan, Q. Li, Q. Feng, C. Zhou, X. Liu, Y. Yang and G. Chen, Energy storage properties and electrical behavior of lead-free $(1 - x)$ $Ba_{0.04}Bi_{0.48}Na_{0.48}TiO_3$–$xSrZrO_3$ ceramics, *J. Mater. Sci.*: *Mater. Electron.* **27**, 3948 (2016).

[38]Z. Yang, H. Du, L. Jin, Q. Hu, S. Qu, Z. Yang, Y. Yu, X. Wei and Z. Xu, A new family of sodium niobate-based dielectrics for electrical energy storage applications, *J. Eur. Ceram. Soc.* **39**, 2899 (2019).

[39]Y. Zhao, J. Xu, C. Zhou, C. Yuan, Q. Li, G. Chen, H. Wang and L. Yang, High energy storage properties and dielectric behavior of $(Bi_{0.5}Na_{0.5})_{0.94}Ba_{0.06}Ti_{1–x}(Al_{0.5}Nb_{0.5})_xO_3$ lead-free ferroelectric ceramics, *Ceram. Int.* **42**, 2221 (2016).

[40]V. S. Puli, D. K. Pradhan, D. B. Chrisey, M. Tomozawa, G. L. Sharma, J. F. Scott and R. S. Katiyar, Structure, dielectric, ferroelectric, and energy density properties of $(1 - x)$BZT–xBCT ceramic capacitors for energy storage applications, *J. Mater. Sci.* **48**, 2151 (2013).

[41]Z. Yu, Y. Liu, M. Shen, H. Qian, F. Li and Y. Lyu, Enhanced energy storage properties of $BiAlO_3$ modified $Bi_{0.5}Na_{0.5}TiO_3$–$Bi_{0.5}K_{0.5}$-TiO_3 lead-free antiferroelectric ceramics, *Ceram. Int.* **43**, 7653 (2017).

[42]X. Liu, H. Yang, F. Yan, Y. Qin, Y. Lin and T. Wang, Enhanced energy storage properties of $BaTiO_3$-$Bi_{0.5}Na_{0.5}TiO_3$ lead-free ceramics modified by $SrY_{0.5}Nb_{0.5}O_3$, *J. Alloys Compd.* **778**, 97 (2019).

[43]X. Qiao, D. Wu, F. Zhang, M. Niu, B. Chen, X. Zhao, P. Liang, L. Wei, X. Chao and Z. Yang, Enhanced energy density and thermal stability in relaxor ferroelectric $Bi_{0.5}Na_{0.5}TiO_3$-$Sr_{0.7}Bi_{0.2}TiO_3$ ceramics, *J. Eur. Ceram. Soc.* **39**, 4778 (2019).

[44]X. Zhao, W. Bai, Y. Ding, L. Wang, S. Wu, P. Zheng, P. Li and J. Zhai, Tailoring high energy density with superior stability under low electric field in novel $(Bi_{0.5}Na_{0.5})TiO_3$-based relaxor ferroelectric ceramics, *J. Eur. Ceram. Soc.* **40**, 4475 (2020).

[45]Z. Yang, H. Du, S. Qu, Y. Hou, H. Ma, J. Wang, J. Wang, X. Wei and Z. Xu, Significantly enhanced recoverable energy storage density in potassium–sodium niobate-based lead free ceramics, *J. Mater. Chem. A* **4**, 13778 (2016).

[46]Q. Yuan, S. Zhan, Y. Li, Y. Wang, H. Yang, J. Zhou, Z. Li, H. Jing, F. Yao and T. Lei, Toward high-end lead-free ceramics for energy storage: $Na_{0.5}Bi_{0.5}TiO_3$-based relaxor ferroelectrics with simultaneously enhanced energy density and efficiency, *Mater. Today Energy* **31**, 101202 (2023).

[47]X. Dong, X. Li, X. Chen, H. Chen, C. Sun, J. Shi, F. Pang and H. Zhou, High energy storage density and power density achieved simultaneously in $NaNbO_3$-based lead-free ceramics via antiferroelectricity enhancement, *J. Materiomics* **7**, 629 (2021).

[48]H. Chen, X. Chen, J. Shi, C. Sun, X. Dong, F. Pang and H. Zhou, Achieving ultrahigh energy storage density in $NaNbO_3$–$Bi(Ni_{0.5}Zr_{0.5})O_3$ solid solution by enhancing the breakdown electric field, *Ceram. Int.* **46**, 28407 (2020).

[49]D. Li, Z. Shen, Z. Li, W. Luo, X. Wang, Z. Wang, F. Song and Y. Li, *P–E* hysteresis loop going slim in $Ba_{0.3}Sr_{0.7}TiO_3$-modified $Bi_{0.5}Na_{0.5}TiO_3$ ceramics for energy storage applications, *J. Adv. Ceram.* **9**, 183 (2020).

[50]X. Li, X. Hao, S. An, Y. Li and Q. Zhang, Enhanced energy storage in Sn-doped sodium bismuth titanate lead-free relaxor ferroelectric ceramics, *J. Mater. Sci.*: *Mater. Electron.* **33**, 5265 (2022).

[51]X. Tong, M. Song, J. Zhou, K. Wang, C. Guan, H. Liu and J. Fang, Enhanced energy storage properties in Nb-modified $Bi_{0.5}Na_{0.5}$-TiO_3–$SrTiO_3$ lead-free electroceramics, *J. Mater. Sci.: Mater. Electron.* **30**, 5780 (2019).

[52]R. Shi, Y. Pu, W. Wang, X. Guo, J. Li, M. Yang and S. Zhou, A novel lead-free $NaNbO_3$–$Bi(Zn_{0.5}Ti_{0.5})O_3$ ceramics system for energy storage application with excellent stability, *J. Alloys Compd.* **815**, 152356 (2020).

[53]X. Ren, L. Jin, Z. Peng, B. Chen, X. Qiao, D. Wu, G. Li, H. Du, Z. Yang and X. Chao, Regulation of energy density and efficiency in transparent ceramics by grain refinement, *Chem. Eng. J.* **390**, 124566 (2020).

[54]Z. Liu, Z. Tang, S. Hu, D. Yao, F. Sun, D. Chen, X. Guo, Q. Liu, Y. Jiang and X. Tang, Excellent energy storage density and efficiency in lead-free Sm-doped $BaTiO_3$–$Bi(Mg_{0.5}Ti_{0.5})O_3$ ceramics, *J. Mater. Chem. C* **8**, 13405 (2020).

[55]M. Li, M. Zhu, M. Zheng, Y. Hou, J. Wang, X. Chao, Z. Yang, J. Zhou, K. Wang and X. Ke, Excellent energy storage and discharge performances in $Na_{1/2}Bi_{1/2}TiO_3$-based ergodic relaxors by enlarging the $[AO_{12}]$ cages, *J. Mater. Chem. C* **10**, 8845 (2022).

[56]L. Wu, Y. Huan, X. Wang, C. Li, Y. Luo and T. Wei, A combinatorial improvement strategy to enhance the energy storage performances of the KNN-based ferroelectric ceramic capacitors, *J. Mater. Sci.* **57**, 15876 (2022).

[57]Z. Liu, M. Li, Z. Tang and X. Tang, Enhanced energy storage density and efficiency in lead-free $Bi(Mg_{1/2}Hf_{1/2})O_3$-modified $BaTiO_3$ ceramics, *Chem. Eng. J.* **418**, 129379 (2021).

[58]J. Wu, A. Mahajan, L. Riekehr, H. Zhang, B. Yang, N. Meng, Z. Zhang and H. Yan, Perovskite $Sr_x(Bi_{1–x}Na_{0.97–x}Li_{0.03})_{0.5}TiO_3$ ceramics with polar nano regions for high power energy storage, *Nano Energy* **50**, 723 (2018).

[59]J. Shi, X. Liu and W. Tian, High energy-storage properties of $Bi_{0.5}Na_{0.5}TiO_3$-$BaTiO_3$-$SrTi_{0.875}Nb_{0.1}O_3$ lead-free relaxor ferroelectrics, *J. Mater. Sci. Technol.* **34**, 2371 (2018).

[60]T. Tunkasiri and G. Rujijanagul, Dielectric strength of fine grained barium titanate ceramics, *J. Mater. Sci. Lett.* **15**, 1767 (1996).

[61]A. Young, G. Hilmas, S. C. Zhang and R. W. Schwartz, Effect of liquid-phase Sintering on the breakdown strength of Barium titanate, *J. Am. Ceram. Soc.* **90**, 1504 (2007).

[62]X. Qiao, X. Zhang, D. Wu, X. Chao and Z. Yang, Influence of Bi nonstoichiometry on the energy storage properties of 0.93KNN–0.07Bi_xMN relaxor ferroelectrics, *J. Adv. Dielectr.* **8**, 1830006 (2018).

[63]J. Shi, X. Chen, X. Li, J. Sun, C. Sun, F. Pang and H. Zhou, Realizing ultrahigh recoverable energy density and superior charge–discharge performance in $NaNbO_3$-based lead-free ceramics

via a local random field strategy, *J. Mater. Chem. C* **8**, 3784 (2020).
[64]P. Zhao, Z. Cai, L. Wu, C. Zhu, L. Li and X. Wang, Perspectives and challenges for lead-free energy-storage multilayer ceramic capacitors, *J. Adv. Ceram.* **10**, 1153 (2021).
[65]S. M. Yang, J. Y. Jo, T. H. Kim, J.-G. Yoon, T. K. Song, H. N. Lee, Z. Marton, S. Park, Y. Jo and T. W. Noh, AC dynamics of ferroelectric domains from an investigation of the frequency dependence of hysteresis loops, *Phys. Rev. B* **82**, 174125 (2010).
[66]L. Yang, X. Kong, Z. Cheng and S. Zhang, Ultra-high energy storage performance with mitigated polarization saturation in lead-free relaxors, *J. Mater. Chem. A* **7**, 8573 (2019).